HHS Public Access

Author manuscript

Mol Cancer Ther. Author manuscript; available in PMC 2016 December 01.

Published in final edited form as:

Mol Cancer Ther. 2015 December ; 14(12): 2850–2863. doi:10.1158/1535-7163.MCT-15-0237.

Potentiation of carboplatin-mediated DNA damage by the Mdm2 modulator Nutlin-3a in a humanized orthotopic breast-to-lung metastatic model

Eva Tonsing-Carter[1], **Barbara J. Bailey**[2,3], **M. Reza Saadatzadeh**[3,4], **Jixin Ding**[3,4], **Haiyan Wang**[3], **Anthony L. Sinn**[2], **Kacie M. Peterman**[2], **Tiaishia K. Spragins**[2], **Jayne M. Silver**[2], **Alyssa A. Sprouse**[3], **Taxiarchis M. Georgiadis**[5], **T. Zachary Gunter**[5,*], **Eric C. Long**[5], **Robert E. Minto**[5], **Christophe C. Marchal**[3], **Christopher N. Batuello**[3], **Ahmad R. Safa**[1], **Helmut Hanenberg**[3,6,7], **Paul R. Territo**[8], **George E. Sandusky**[9], **Lindsey D. Mayo**[3,10], **Christine M. Eischen**[11], **Harlan E. Shannon**[3], and **Karen E. Pollok**[1,2,3]

[1]Department of Pharmacology and Toxicology, Indiana University School of Medicine, Indianapolis, IN 46202, USA

[2]*In Vivo* Therapeutics Core, Indiana University Melvin and Bren Simon Cancer Center, Indiana University School of Medicine, Indianapolis, IN 46202, USA

[3]Department of Pediatrics, Herman B Wells Center for Pediatric Research, Indiana University School of Medicine, Indianapolis, Indiana 46202, USA

[4]Goodman Campbell Brain and Spine, Department of Neurosurgery, Indiana University School of Medicine, Indianapolis, IN 46202, USA

[5]Department of Chemistry and Chemical Biology, Indiana University-Purdue University Indianapolis, Indianapolis, IN 46202, USA

[6]Department of Medical & Molecular Genetics, Indiana University School of Medicine, Indianapolis, Indiana 46202, USA

[7]Department of Otorhinolaryngology and Head/Neck Surgery, Heinrich Heine University, Düsseldorf, Germany

[8]Indiana Institute for Biomedical Sciences Imaging, Department of Radiology, Indiana University School of Medicine, Indianapolis, IN 46202, USA

[9]Department of Pathology, Indiana University School of Medicine, Indianapolis, IN 46202, USA

[10]Department of Biochemistry and Molecular Biology, Indiana University School of Medicine, Indianapolis, IN 46202, USA

[11]Department of Pathology, Microbiology and Immunology, Vanderbilt University Medical Center, Nashville, TN 37232, USA

Corresponding Author: Karen E. Pollok, Herman B Wells Center for Pediatric Research, 1044 W. Walnut St, R4-302, Indiana University Simon Cancer Center, Indianapolis, Indiana 46202. Phone: 317-274-8891; Fax: 317-278-9298; kpollok@iu.edu.

*Current Address: T. Zachary Gunter, Eli Lilly and Company, Product Design and Developability, Indianapolis, Indiana

Conflict of Interest Statement: No potential conflicts of interest were disclosed.

Abstract

Triple-negative breast cancers (TNBCs) are typically resistant to treatment, and strategies that build upon frontline therapy are needed. Targeting the murine double minute 2 (Mdm2) protein is an attractive approach as Mdm2 levels are elevated in many therapy-refractive breast cancers. The Mdm2 protein-protein interaction inhibitor Nutlin-3a blocks the binding of Mdm2 to key signaling molecules such as p53 and p73α, and can result in activation of cell-death signaling pathways. In the present study, the therapeutic potential of carboplatin and Nutlin-3a to treat TNBC was investigated, as carboplatin is under evaluation in clinical trials for TNBC. In mutant p53 TMD231 TNBC cells, carboplatin and Nutlin-3a led to increased Mdm2 and was strongly synergistic in promoting cell death *in vitro*. Furthermore, sensitivity of TNBC cells to combination treatment was dependent on p73α. Following combination treatment, γH2AX increased and Mdm2 localized to a larger degree to chromatin compared to single-agent treatment, consistent with previous observations that Mdm2 binds to the Mre11/Rad50/Nbs1 complex associated with DNA and inhibits the DNA-damage response. *In vivo* efficacy studies were conducted in the TMD231 orthotopic mammary fat pad model in NOD.Cg-Prkdc^{scid}Il2rg^{tm1Wjl}/SzJ (NSG) mice. Using an intermittent dosing schedule of combined carboplatin and Nutlin-3a, there was a significant reduction in primary tumor growth and lung metastases compared to vehicle and single-agent treatments. Additionally, there was minimal toxicity to the bone marrow and normal tissues. These studies demonstrate that Mdm2 holds promise as a therapeutic target in combination with conventional therapy and may lead to new clinical therapies for TNBC.

Keywords

Breast cancer; Animal models of cancer; Noninvasive imaging in animal models; Other tumor suppressor genes; Combination chemotherapy; Xenograft models; Cellular responses to anticancer drugs; Modulation of DNA repair; Reversal of drug resistance; Preclinical toxicology; Mdm2; carboplatin; p73

Introduction

The development of efficacious therapies for TNBC has been challenging due to its aggressive nature and lack of hormone receptors that can be therapeutically targeted (1, 2). Platinum agents, such as cisplatin and carboplatin, form DNA-platinum adducts resulting in intra- and interstrand DNA crosslinks leading to increased double strand breaks and cell death (3). Clinical studies have indicated that platinum-based therapy can provide enhanced efficacy in TNBC (4, 5). Furthermore, clinical trials are currently evaluating the utility of combination therapies that include carboplatin to specifically treat TNBCs with metastases (NCT01881230, NCT00691379, and NCT01281150; www.clinicaltrials.gov). While platinum agents show promise in the clinic, new combination treatment modalities are needed that optimize tumor cell kill without enhancing platinum-mediated toxicity to normal tissues, thereby increasing the therapeutic window.

Targeting the mouse double minute 2 (Mdm2) signaling axis holds promise as a novel approach to combination therapy in the treatment of TNBC. Mdm2 is a multi-faceted protein involved in numerous aspects of cell growth, survival, and invasion (6). Mdm2 is a E3

ubiquitin ligase that targets p53 for degradation by the proteasome (7) and is expressed in a number of tumor types. There is mounting evidence demonstrating the critical role Mdm2 plays in cell growth regulation and cancer (6). In breast cancers, studies have shown *Mdm2* gene amplifications range from 10–60% with some studies indicating a worse prognosis with overexpression of Mdm2 or gene amplification (6, 8). Moreover, evidence suggests that high Mdm2 levels correlate with a higher incidence of metastasis *in vivo* (6, 8, 9).

Nutlin-3a is a small molecule, which binds to the N-terminal hydrophobic pocket of Mdm2 and blocks protein-protein interactions (PPIs) between Mdm2 and p53 (10). Nutlin-3a also inhibits the binding of the p73 isoform p73α, as well as E2F1 and hypoxia inducible factor 1α (Hif-1α), to the N-terminal hydrophobic pocket of Mdm2 (11–13). It is estimated that p53 is mutated in approximately 50% of all cancers with 60% of TNBCs bearing mutations in p53 (14, 15); in contrast, p73 is rarely mutated in cancers (14, 16). p73 is a member of the p53 family of tumor suppressors and has similar transactivation functions relating to the induction of pro-apoptotic genes in response to cellular stress (17, 18). Lau and colleagues showed that when cells were treated with Nutlin-3a, the binding of p73α to Mdm2 was inhibited, leading to p73α-mediated induction of pro-apoptotic downstream targets and increased apoptosis in cells lacking wild-type p53 (12). The use of Nutlin-3a to inhibit PPIs between Mdm2 and binding partners, including p53, p73α, E2F1, and Hif-1α (10–13), may lead to a multi-targeted approach to treating cancer, especially when coupled with clinically relevant DNA damaging drugs such as carboplatin.

The purpose of the present study was to investigate the therapeutic potential of modulating Mdm2 function in the context of carboplatin-mediated DNA damage utilizing an optimized human mutant p53 TNBC orthotopic xenograft model. *In vitro*, carboplatin and Nutlin-3a were strongly synergistic in increasing cell death in TNBC cells with a mutant p53 background. siRNA studies indicated that drug sensitivity, as well as Mdm2 protein levels, were dependent on p73α. Following combination treatment in our model system, there was increased Mdm2 localized to chromatin compared to single agent treatment. *In vivo* efficacy experiments, conducted in the TMD231 orthotopic mammary fat pad model in NOD.Cg-Prkdc^{scid}Il2rg^{tm1Wjl}/SzJ (NSG) mice, demonstrated a statistically significant reduction in primary tumor volume as well as lung metastases with significantly increased probability of survival compared to vehicle and single-agent treatments. In regards to normal tissue toxicity, body weights were only transiently affected, and recovered to normal levels post-treatment. Treatment-mediated decreases in hematopoietic function were similar in mice treated with carboplatin alone or combination Nutlin-3a/carboplatin, and these decreases did not lead to bone marrow aplasia. The present study demonstrates that Mdm2 is a valid therapeutic target in mutant p53 TNBC and that Mdm2 PPI inhibitors offer new avenues for exploring novel combination therapies for treatment of TNBC.

Materials and Methods

Cells and Cell Culture

MDA-MB-231 (HTB-26), MDA-MB-468 (HTB-132), MCF10A (CRL-10317), and MCF-7 (HTB-22) were purchased from ATCC in 2010 (MCF-7), 2012 (MDA-MB-468), and 2014 (MDA-MB-231 and MCF10A). Primary human fibroblast cells were kindly provided by

Kathrin Scheckenbach, Düsseldorf, Germany in 2014. TMD231 cells were obtained from Dr. Harikrishna Nakshatri in 2009 and are a derivative of the MDA-MB-231 cell line (19). TMD231 cells were transduced with E2-Crimson lentiviral vector, p2CL7CR2wo, (TMD231-CR) for *in vivo* imaging as described (20). Upon receipt, cell stocks were cryopreserved at low passage. Authentication of molecular profiles was verified by short tandem repeat (STR) analysis (IDEXX BioResearch), and cells tested negative for mycoplasma. TMD231 cells were cultured in MEM-α (Gibco) supplemented with 10% FBS (Atlanta Biologicals) and 1% HEPES (Invitrogen). MDA-MB-231, MDA-MB-468, and primary human fibroblast cells were cultured in DMEM (Gibco) supplemented with 10% FBS (Atlanta Biologicals). MCF10A cells were cultured in Medium 171 (Gibco) supplemented with 1% MEGS (Invitrogen) and 0.1% cholera toxin (Sigma). All cells were cultured at 37°C with 5% CO_2.

Compounds

Nutlin-3a was synthesized at the IUPUI Chemical Synthesis and Organic Drug Lead Development Core and confirmed through HPLC-MS analysis. Carboplatin was purchased from Sigma. For *in vitro* studies, carboplatin was dissolved in H_2O, while Nutlin-3a was dissolved in DMSO. Final concentration of DMSO was <0.2%. For *in vivo* studies, carboplatin was dissolved in PBS, while Nutlin-3a was suspended in 0.5% methylcellulose (Sigma) and 0.05% Tween80 (Sigma).

Methylene Blue Proliferation Assay

The methylene blue proliferation assay was derived from Oliver *et al*. (21). Cells were treated with varying concentrations of Nutlin-3a, carboplatin, or combination dose-ratios for 3–5 days in triplicate-sextuplicate. IC_{50} values were calculated according to the linearization method of Chou and Talalay (22) and were used to construct isobolograms as previously described (23).

Clonogenic Proliferation Assay

TMD231 cells were plated at low cell density and treated with Nutlin-3a, carboplatin, or a 1:1 combination and colonies enumerated at Day 14.

Cell Counting Proliferation Assay

Cells were treated with Nutlin-3a, carboplatin, 1:1 Nutlin-3a/carboplatin, or appropriate vehicle control. Each experiment was conducted in triplicate. The number of live cells was determined in the presence of trypan blue dye via hemocytometer.

In Vitro Analysis of Activated Caspase-3/7, γH2AX, Mdm2, and Cleaved PARP

For *in vitro* studies, activated Caspase-3/7 was measured using ApoTox-Glo Triplex Assay (Promega) as per manufacturer's instructions. For measurement of γH2AX foci, TMD231 cells were seeded on chamber slides (Lab-Teck Brand Products) and treated the next day. Cells were fixed with 2% paraformaldehyde, and stained with a fluorescein isothiocyanate (FITC)-conjugated phospho-histone H2AX (Ser139) primary antibody (1:200 dilution, Cell Signaling), incubated with 4',6-diamidino-2-phenylindole (DAPI), and analyzed as

described in the Supplemental Materials and Methods. γH2AX, Mdm2, and cleaved PARP were measured using MILLIPLEX MAP γH2AX/β-Tubulin, Mdm2/β-Tubulin or PARP/GAPDH Magnetic Beads (EMD Millipore) as per manufacturer's instructions. Mean fluorescence intensities (MFI) per μg protein were normalized to GAPDH or β-Tubulin MFI.

Annexin V and 7-AAD Apoptosis Assay

TMD231 cells were treated for 96 hours with the IC_{50} concentrations of carboplatin or Nutlin-3a alone, or in 1:0.3, 1:1, or 1:3 dose-ratios of Nutlin-3a:carboplatin in triplicate. Cells were collected and stained using Annexin V-FITC (BD Biosciences) and 7-AAD (BD Biosciences) per manufacturer's instructions and analyzed by flow cytometry.

Western Blot Analysis

Cells were lysed with RIPA buffer containing 1 Complete-EDTA free mini tablet (Roche), and 1% phosphatase inhibitor 3 (Sigma) (24, 25). Protein was quantified using the DC Protein Assay (Bio-Rad) per manufacturer's instructions. Western blot densitometry was determined using ImageJ software (http://imagej.nih.gov/) and proteins of interest were normalized to loading control and expressed relative to untreated, vehicle, or siControl cells.

Antibodies

For *in vitro* and *in vivo* Western blots, Mdm2 (90kDa band) antibody cocktail included SMP14 (sc-965, Santa Cruz), 2A9 (OP155T, Calbiochem), and 4B11 (OP143, Calbiochem). Antibodies for PUMA (21kDa, #4976, Cell Signaling), p21 (21kDa, DCS60, Cell Signaling), p53, (DO-1, sc-126, Santa Cruz), MdmX (55kDa, ab154324, Abcam), γH2AX (17kDa, #2577, Cell Signaling), α-tubulin (50 kDa, clone B-5-1-2, Sigma-Aldrich) and GAPDH (37kDa, 14C10, #2118, Cell Signaling) were also used. In the TMD231 cells, the predominant form of p73 detected was the alpha isoform (~80kDa, A300-126A, Bethyl Laboratories). While the p73 polyclonal antibody A300-126A recognizes multiple isoforms of p73, it does not recognize ΔNp73. For the chromatin association assay, antibodies included Mdm2 (3G9, Millipore), H2AX (A300-082A, Bethyl), and β-Actin (AC-15, Sigma) as previously described (25).

Transient knockdown of p73α with siRNA

ON-TARGET*plus* non-targeting control and SMARTpool ON-TARGET*plus* p73 siRNAs were purchased from Dharmacon (GE Healthcare). See Supplemental Materials and Methods for p73 siRNA constructs. Lipofectamine RNAiMAX (Life Technologies) was used for transfection. For Western blot and proliferation assays, TMD231 cells were transfected with either non-targeting control siRNA or p73 siRNA. On day 1 post-transfection, cells were seeded into 6-well plates (Western) or 96-well plates (proliferation assays), treated with Nutlin-3a or carboplatin, alone or in combination for 72 hours, and IC_{50} values determined. For Western blot experiments, cells were treated with Nutlin-3a or carboplatin, alone or in combination for 24 hours.

Chromatin Association Assay

TMD231 cells were treated with Nutlin-3a, carboplatin, 1:1 combination, or vehicle control for 6 hours. Cells were harvested, and soluble and chromatin bound proteins separated with CSK buffer as described (26). The chromatin fraction was extracted with RIPA buffer containing protease inhibitors (24, 25). Whole cell lysates were prepared as previously reported (27).

Animals

All studies were carried out in accordance with, and approval of, the Institutional Animal Care and Use Committee of Indiana University School of Medicine and the Guide for the Care and Use of Laboratory Animals. Female NOD/scid and NOD.Cg-*Prkdc*^{scid}Il2rg^{tm1Wjl}/SzJ (NSG) mice 6–8 weeks of age were obtained from the *In Vivo* Therapeutics Core of the Indiana University Simon Cancer Center. Animals were maintained under pathogen-free conditions and maintained on Irradiated Global 2018 (Uniprim 4100 ppm) (TD.06596, Harlan Laboratories USA) food pellets with *ad libitum* access to autoclaved, acidified tap water under a 12-hour light-dark cycle at 22–24°C.

Animal Strain Comparisons

NOD/scid and NSG mice were implanted with 1×10^6 TMD231 cells into the mammary fat pad. Tumor volumes were calculated according to the formula $(\alpha^2 \times \beta)/2$, where α was the shorter and β was the longer of the two dimensions following caliper measurements. Mice were sacrificed throughout the study to better understand longitudinal metastasis formation in the lungs via H&E staining.

Orthotopic Xenograft Studies

In the first study, NSG mice were implanted with 1×10^6 TMD231 or TMD231-CR cells in the mammary fat pad. Mice were optically imaged on day 7 and block-randomized to treatment groups based on tumor fluorescence intensity: vehicle (Veh; PBS +methylcellulose/Tween80), 25 mg/kg carboplatin i.p. (Carb) (in AM), 200 mg/kg Nutlin-3a p.o. (Nut) (in PM), or 25 mg/kg carboplatin+200 mg/kg Nutlin-3a (Combo), and were dosed three times weekly for 2 weeks. Body weights were collected weekly and primary tumors were measured via caliper bi-weekly. The endpoint for the study was when the primary tumors reached $\geq 1000 mm^3$. At the time of sacrifice, the primary tumors and lungs were collected for Ki67 and H&E staining.

In the second study, animals were implanted and block-randomized into treatment groups: vehicle (Veh; PBS+methylcellulose/Tween80), 20 mg/kg carboplatin (Carb), 200 mg/kg Nutlin-3a (Nut), and 20 mg/kg carboplatin+200 mg/kg Nutlin-3a combination (Combo) (n=12 per group). Mice were dosed twice weekly for 4 weeks. Body weights and primary tumors were measured as described above. To determine drug effects on bone marrow, four mice from each treatment group were sacrificed at 5 days following the completion of treatment and total bone marrow cell counts determined. At the time of sacrifice, the primary tumors and lungs were collected and fixed for H&E analysis. Femurs were collected to determine bone marrow cellularity. The remaining mice from each treatment group (n=8

per group) were used to examine the probability of survival for tumors to reach ≥800 mm^3. Total bone marrow cell counts were also determined at the endpoint (n=3 per group).

In the third study, mice were implanted as described above and dosed with vehicle (Veh; PBS+methylcellulose/Tween80), 20 mg/kg carboplatin (Carb) (in AM), 200 mg/kg Nutlin-3a (Nut) (in PM), or 20 mg/kg carboplatin+200 mg/kg Nutlin-3a in combination (Combo) twice weekly for 4 weeks. Endpoint was when primary tumors reached ≥1000 mm^3. Following necropsy, primary tumors, lungs, liver, spleen and femur bones were collected and evaluated with H&E staining. Bone marrow cellularity, complete blood counts (CBCs), and progenitor assays were completed.

Tissue Processing and Staining

Tissues were fixed in 10% neutral buffered formalin at 4°C for 24 hours followed by tissue processing, and then embedded in paraffin. Five-micron sections were cut and stained for routine H&E or Ki67 (DAKO).

Whole Slide Digital Imaging

The Aperio ScanScope CS system whole slide digital imaging system was used for imaging (Leica Biosystems). All slides were imaged at 20×. Images were captured from the whole slides and stored in the Spectrum software system. See Supplemental section for details of analysis.

In Vivo Imaging

Anesthesia was induced with 4–5% isoflurane (balance medical oxygen), and maintained with 1–2% isoflurane. Mice were imaged using an Optix MX3 (ART Technologies), where excitation and emission of E2-Crimson was carried out at 635 nm and 650 nm, respectively.

Bone Marrow Cellularity

Femurs were collected, crushed, and cells were filtered through 70 μm filters. Red blood cells were depleted with RBC Lysis Buffer (Qiagen). Total cell counts were determined using a Beckman Coulter Counter.

Colony-forming Unit Progenitor Assay

Bone marrow cells were plated in triplicate at 2×10^4 per plate in MethoCult GF M3434 (StemCell Technologies) and progenitor colonies counted as described in Cai *et al*. (28).

Total Complete Blood Counts (CBCs)

Tumor-bearing mice were treated with vehicle control (Veh), carboplatin (Carb), Nutlin-3a (Nut) or carboplatin+Nutlin-3a combination (Combo). After a 2–4 week recovery period, an aliquot of peripheral blood was analyzed via Hemavet for red blood cells, platelets, and white blood cells.

Statistics

Data were analyzed by one-, two-way, or repeated measures ANOVA or Student's t-test, as appropriate, using SigmaPlot 11.2 (Systat Software, Inc.). In order to normalize the variability, data were logarithmically transformed for the purposes of statistical analysis for the MILLIPLEX data, Ki67 and H&E stain quantification, and CBCs data. Differences among individual pairs of means were determined by the Holm-Sidak post-hoc test. IC_{50} were values determined using CalcuSyn (BioSoft). Kaplan-Meier survival plots were generated using SigmaPlot, and changes in survival analyzed by log-rank test. Data were considered significant at $p<0.05$. Data are presented as mean±1SD unless noted otherwise.

Results

In vitro evaluation of carboplatin and Nutlin-3a on growth of mutant p53 TNBC cells

The effects of single or combination Nutlin-3a/carboplatin treatment was evaluated in a panel of TNBC cell lines using methylene blue proliferation assays. Both carboplatin and Nutlin-3a produced dose-related decreases in cell proliferation in MDA-MB-231, TMD231, and MDA-MB-468 cells (Fig. 1A–C). Further, the IC_{50} values for both drugs were greatly reduced in combination treatments compared to single-agent treatments (Supplemental Table S1). In the isobologram analyses, the isoboles of different dose-ratios of carboplatin and Nutlin-3a fell well below the line of additivity indicating a synergistic effect of combination treatments (Fig. 1E–G). In addition, combination indices were <1 for all Nutlin-3a:carboplatin ratios tested, again indicating synergism between Nutlin-3a and carboplatin (Supplemental Fig. S1). As expected, MCF-7 (wt-p53) cells were more sensitive to single agent Nutlin-3a (Fig. 1D), and isobologram analysis indicated Nutlin-3a was synergistic with carboplatin (Fig. 1H). Additionally, combination indices <1 were observed in MCF-7 cells (Supplemental Figure S1).

Effects of combination treatment on cell death in TNBC cells and normal cells *in vitro*

Based on proliferation assay results, the effect of combination treatment on clonogenicity was evaluated in TMD231 cells. Colony formation was inhibited in a concentration-dependent manner following Nutlin-3a, carboplatin, and 1:1 combination treatment (Fig. 2A–C). Growth was inhibited by ~50% at concentrations of 2.5 μM carboplatin or 30 μM Nutlin-3a alone (Fig. 2A–B). In contrast, following combination treatment, clonogenic growth was inhibited ~50% by 1.5 μM of each compound, consistent with synergism (Fig. 2C). To understand how cell proliferation was inhibited, kinetic experiments were conducted using TMD231 cells to quantify the number of viable cells throughout a 5-day treatment period. We elected to use a 1:1 dose-ratio of Nutlin-3a:carboplatin for this study since this ratio exhibited the largest synergism in the isobologram analysis (Fig. 1F). Based on analysis of carboplatin plasma levels in clinical trials for metastatic disease, a concentration of 15 μM carboplatin was selected for the *in vitro* studies (29). Consistent with our cell-proliferation data, 15 μM Nutlin-3a did not markedly affect cell viability, whereas 15 μM of carboplatin significantly reduced cell number, over time (Fig. 2D). For the combination treated cells, there was a significant further reduction in the number of cells relative to carboplatin alone (Fig. 2D, inset).

The sensitivity of MCF10A mammary epithelial and normal human fibroblast cells to single agent and combination treatment was compared to that of TMD231 cells. Cells were exposed to 15 μM of carboplatin, Nutlin-3a, or a 1:1 ratio of carboplatin and Nutlin-3a for 5 days. As expected, wild-type p53 normal human cells were significantly more sensitive to Nutlin-3a than the mtp53 TMD231 cells (Fig. 2E). Interestingly, the TMD231 cells were significantly more sensitive to carboplatin than the normal human cells (Fig. 2E), consistent with previous reports that mtp53 cancer cells can have inefficient nucleotide excision repair (30), rendering them more susceptible to platinum-mediated DNA damage. As observed in Fig. 2D, TMD231 cells were significantly more sensitive to the combination treatment than single agent alone. Moreover, TMD231 cells were significantly more sensitive than the MCF10A epithelial and human fibroblast cells to 15 μM combination treatment (Fig. 2E). While *in vitro* toxicity data do not necessarily predict toxicity *in vivo*, these data indicate that careful selection of compound doses and scheduling will be crucial to avoid unacceptable levels of normal tissue toxicity *in vivo*.

We next examined the effects of the combination treatment on activated Caspase-3/7 following dual Nutlin-3a and carboplatin treatment in TMD231 cells. The 1:1 combination of Nutlin-3a:carboplatin led to a significant increase in activated Caspase-3/7 compared to single drug treatments after 3 days of treatment (Fig. 2F). Additionally, cleaved PARP was significantly increased in combination treated TMD231 cells following 3 days treatment (Fig. 2G). Further, apoptosis was examined in TMD231 cells after 4 days of treatment, based on our observation of reductions in cell number by 4 days post treatment (Fig. 2D, inset). The IC_{50} values from three different dose-ratios [1:1 (0.8:0.8 μM), 1:0.3 (3.75:1.25 μM), and 11:3 (0.7:2.1 μM) Nutlin-3a:carboplatin], as calculated from the TMD231 proliferation assays (Fig. 1 and Supplemental Table S1), were used in the apoptosis assays. Total apoptosis/necrosis was significantly increased in all combination-treatments (50–75%) compared to either drug alone (20–30%) (Fig. 2H), indicating that cell death pathways are activated in TNBC cells following combination treatment *in vitro*. Normal fibroblast cells were relatively resistant to Nutlin-3a and carboplatin both as single agents and in combination with total apoptosis/necrosis <5% (Supplemental Fig. S2) indicating specificity of the combination treatment inducing apoptosis in TNBC cells compared to normal cells.

Target modulation and mechanism of action following combination treatment

We hypothesized, based on previous studies (12), that the effects of Nutlin-3a in a mutant p53 background were most likely attributable to p73α-mediated signaling. To gain an understanding of molecular mechanisms that contribute to cell death in TNBC cells, the effect of treatment on levels of p73α and downstream targets Mdm2, p21, and PUMA was evaluated in TMD231 cells (Fig. 3A). TMD231 cells were transiently transfected with non-targeting control or p73 siRNAs followed by treatment with single agent or combination for 24 hours. In the siControl RNA TMD231 cells, Nutlin-3a alone and combination Nutlin-3a/carboplatin produced increases in Mdm2 when compared to vehicle-treated cells (Figure 3A, left panel). p73α was constitutively expressed in TMD231 cells and no large changes in p73α levels were evident following treatment. PUMA levels were higher in combination-treated TMD231 cells compared to vehicle and single agent-treated cells and increases in p21 were observed following carboplatin or combination treatment. Efficient knockdown of

p73α was obtained (Fig 3A, right panel) and the effect of p73α knockdown following treatment was evaluated. In contrast to siControl cells treated with Nutlin-3a or combination, Mdm2 protein levels were lower in siRNAp73-transfected cells, indicating that p73α plays a role in regulating Mdm2 levels (Fig. 3A). In comparison to siControl cells, p21 levels were lower in carboplatin- and combination-treated siRNAp73 cells and PUMA levels were lower in combination-treated siRNAp73 cells, indicating that p21 and PUMA induction is dependent to some extent on p73α (Fig. 3A). The levels of the Mdm2-binding partner Mdmx were also evaluated; no significant changes in protein levels in both siControl and siRNAp73 transfected cells were observed following treatment (Fig. 3A).

Sensitivity of TMD231 cells to carboplatin and Nutlin-3a was dependent on p73α protein levels. When cellular sensitivity was examined by methylene blue proliferation assays, there was a significant increase in IC_{50} values for carboplatin alone and carboplatin plus Nutlin-3a at a 1:1 dose-ratio in siRNAp73-transfected TMD231 cells compared to siControl transfected cells (Fig. 3B).

Cell cycle analysis indicated that the TMD231 cell line had both diploid and aneuploid subpopulations and that carboplatin-treated TMD231 cells accumulated in S and G2/M in both subpopulations (Supplemental Fig. S3), which is consistent with previous reports that platinum agents lead to S and G2/M accumulation (31). Nutlin-3a alone did not induce cell cycle arrest in mutant p53 TMD231 cells (Supplemental Fig. S3). Additionally, TMD231 cells treated with the 1:1 Nutlin-3a:carboplatin combination arrested in S and G2/M and also exhibited an increased sub-G1 apoptotic population (Supplemental Fig. S3).

Mdm2 can modulate the ability of cells to sense DNA damage through its direct binding to Nbs1 of the MRN DNA repair complex (24). Therefore, we next determined if increased levels of total Mdm2 correlated with increased levels of Mdm2 associated with the chromatin fraction. TMD231 cells were treated with 15 μM Nutlin-3a, 15 μM carboplatin, or 1:1 combination for 6 hours, and the levels of Mdm2 in whole cell lysates and chromatin fraction lysates were determined by Western blot. Following Nutlin-3a or combination treatment, whole cell lysates showed increased levels of Mdm2 (Fig. 3C). In chromatin fractions isolated from the different treatment groups, association of Mdm2 with the chromatin was increased in combination-treated cells compared to the untreated or single agent-treated cells (Fig. 3D). These findings are consistent with the interpretation that the increased localization of Mdm2 to chromatin leads to inhibition of the MRN complex (24), and may decrease the ability of cells to sense carboplatin-mediated DNA damage leading to increased cell death. Time course studies indicated that γH2AX foci were significantly elevated in combination-treated versus single agent- and vehicle-treated cells by 48 hours post-treatment using confocal microscopy as a highly sensitive measure of γH2AX foci formation (Fig. 3E). Analysis of γH2AX via MILLIPLEX indicated significant increases in γH2AX by 72 hours post-treatment (Fig. 3F). Significant increases in Mdm2 were evident in TMD231 cells treated with Nutlin-3a and combination at all time points analyzed (Fig. 3G).

It is possible that blockade of the N-terminal p53-binding site of Mdm2 by Nutlin-3a could result in stabilization of mutant p53 (32). However, in TMD231 cells, there was no increase in mtp53 steady-state protein levels upon treatment with combination Nutlin-3a/carboplatin

compared to vehicle (Fig. 3A). Cycloheximide experiments indicated that mtp53 was highly stable and no differences in mtp53 stability were observed in vehicle- versus combination treated TMD231 cells (Supplemental Fig. S4). Therefore, Nutlin-3a did not have an effect on mtp53 protein levels.

Development of a fluorescence imaging model for early detection of orthotopic TMD231 primary mammary fat pad tumors

To optimize an *in vivo* animal model to study human TNBC, we initially compared the growth kinetics and metastasis to the lung in Nod/Scid versus NSG mice. In contrast to Nod/Scid mice, TMD231 tumors implanted in NSG mice grew more consistently, at a faster rate, and lung metastases were detected earlier following implant (Fig. 4A–B). The NSG strain was thus selected for subsequent studies. In NSG mice, TMD231 fat pad tumors were palpable by day 7 post-implantation, but the tumors were too small to be accurately measured by calipers until approximately day 14 or later, a time point at which tumor burden rapidly increases at both the primary and lung metastatic sites. To optimize the therapeutic window in the model, mice were randomized to treatment groups based on primary tumor size at day 7 using fluorescence imaging.

TMD231-CR transduced cells expressed high levels of E2-Crimson (Supplemental Fig. S5A–B), and fluorescence intensity was linearly related to the number of cells implanted in the mammary fat pad (Supplemental Fig. S5C–D). Further, sensitivity to Nutlin-3a and carboplatin in an *in vitro* proliferation assay, alone or in combination was similar to that observed in non-transduced TDM231 parental cells (Fig. 1B, Supplemental Table S1, and Supplemental Fig. S5E). Fluorescence intensity from tumors was detected in the mammary fat pad as early as 7 days post-implantation in nearly 100% of the mice, which is a time point before detection of metastatic foci in the lungs (Fig. 4A–B) and was used to block-randomize mice into treatment groups at day 7 post-implantation (Supplemental Fig. S5F–G). We also evaluated whether fluorescence imaging could be used to longitudinally monitor the appearance of metastatic foci in the lungs. However, the photon emission from tumor foci in the lungs could not be detected, most likely due to secondary inner-filtering and light scattering by tissue surrounding the foci. Therefore, H&E staining of lung tissue was used to quantify metastatic foci at the end of each study. Using this optimized model, we performed dose-finding studies for carboplatin to identify a dose and schedule to combine with Nutlin-3a. Carboplatin produced dose-related decreases in TMD231-CR growth and increased probability of survival using an endpoint of primary tumor volume $\geq 1000\ mm^3$ (Fig. 4C–D). The median survival was 41±3.6 days for vehicle, 44±4.3 days for 1 mg/kg, 48±1.9 days for 3 mg/kg, and 58±0 days for 30 mg/kg of carboplatin (Fig. 4D). Based on these data, we elected to administer carboplatin at 20 mg/kg in the combination efficacy studies.

In vivo effects of combination Nutlin-3a/carboplatin treatment on growth of primary tumor and metastatic foci in the lung

Combination treatment significantly inhibited primary tumor growth compared to vehicle and single agent treatments (Fig. 5A). Body weights were transiently reduced by carboplatin and the combination of Nutlin-3a/carboplatin; however, by the end of the study, all body

weights were within a normal range (Fig. 5B). In addition, there were no visual signs of dehydration, diarrhea, or hemorrhaging of the gastrointestinal tract. Further, primary tumors excised at the termination of the study weighed significantly less from mice treated with combination therapy compared to vehicle and single agent treatments (Fig. 5C). Additionally, there was a significant reduction in Ki67 staining in primary tumors of combination treated mice as measured by whole slide digital imaging (Fig. 5D).

At termination of the study, the metastatic burden in the lungs was compared among the treatment groups (Fig. 5E–F). In contrast to mice treated with vehicle or single-agent, the combination treatment significantly decreased the metastatic burden as measured by H&E staining and whole slide digital imaging analysis (Fig. 5F). From the present data, it is not clear whether the combination treatment kills metastatic cells at the primary tumor site, inhibits the metastatic process, and/or leads to tumor cell death after the TMD231 cells metastasize to the lungs. *In vitro* invasion assays however, indicated that the combination treatment did not significantly affect cell invasion when compared to vehicle- or single agent-treatments (Supplemental Fig. S6).

To evaluate potential pharmacodynamic (PD) biomarkers of therapeutic response *in vivo*, NSG mice were implanted with TMD231-CR cells and treated for 3 consecutive days with vehicle, carboplatin, Nutlin-3a, or Nutlin-3a/carboplatin combination. The tumors were excised 2 hours after the last dose and tumor lysates examined by Western blot (Supplemental Fig. S7A–B). In PD study 1, tumors were lysed in 1% SDS to efficiently isolate nuclear-localized proteins (Supplemental Fig. S7A). Basal levels of p73α did not significantly change in any of the groups. While Mdm2 levels were overall higher in tumors from the Nutlin-3a treated group versus vehicle, it was not significant ($p=0.08$). In comparison to the carboplatin-alone treated group, Mdm2 levels were significantly higher in the Nutlin3a-alone and combination treated groups ($p<0.05$). Furthermore, p21 levels significantly increased in tumors from mice treated with the combination compared to vehicle ($p<0.05$). In PD study 2, the tumor samples were lysed in RIPA buffer since we have found that this extraction method is optimal for detection of the phosphoprotein γH2AX in tumor tissue (Supplemental Fig. S7B). Analysis of Western blots via densitometry indicated that while γH2AX increased in the single agent- and combination-treated tumors compared to vehicle-treated mice, statistical significance was not reached ($p>0.05$); mutant p53 levels remained unchanged across the treatment groups (Supplemental Fig. S7B). In addition, the levels of activated Caspase-3 and cleaved PARP were evaluated in tumor lysates derived from PD study 2. While activated Caspase-3 was detectable in 50% of the vehicle-treated tumors, activated Caspase-3 was detected in 100% of the tumors treated with Nutlin-3a, carboplatin, or combination (Supplemental Fig. S7C). Similar results were obtained in tumor samples probed for cleaved PARP with 100% of tumors having measureable levels of cleaved PARP following combination treatment while only 50–66% of tumors contained measureable levels of cleaved PARP following vehicle, Nutlin-3a, or carboplatin treatment (Supplemental Fig. S7D).

Effects of combination Nutlin-3a/carboplatin treatment on survival and normal tissue toxicity *in vivo*

To confirm therapeutic effects on tumor growth and evaluate effects of treatment on hematopoiesis, a sensitive indicator of normal tissue toxicity, a second orthotopic study was conducted. Similar to the previous study (Fig. 5), the combination treatment led to significantly reduced tumor volumes when compared to vehicle and single agent treatments (Fig. 6A) with only a transient decrease in body weights during therapy (Fig. 6B). Significant reductions in metastatic burden following combination treatment were also observed (Fig. 6C). Survival was evaluated using the day post-implant at which the primary tumor volume reached ≥800 mm^3 as the survival endpoint. In contrast to single-agent therapy, the Nutlin-3a/carboplatin combination significantly increased the probability of survival (Fig. 6D). Median survival was 40±1.5 days for vehicle, 40±8.1 for Nutlin-3a, 47±2.6 for carboplatin, and 54.3±0.9 days for the combination (Fig. 6D). Bone marrow cellularity was determined at 5 days and ≥14 days post-treatment. At 5 days post-treatment, total bone marrow cell counts (Fig. 6E, left panel) were significantly reduced in combination-treated mice relative to the other groups. However, by 14–28 days post-treatment (Recovery), bone marrow cellularity had recovered to control levels (Fig. 6E, right panel).

Normal tissue toxicity was further examined in a third study. Total bone marrow cell counts were analyzed following a 2-week recovery period post treatment in all groups, and the frequency of hematopoietic progenitor cells in the bone marrow was evaluated. While complete blood counts and hematopoietic progenitors were significantly decreased in samples from mice treated with carboplatin alone or the combination compared to vehicle or Nutlin-3a alone, there were no differences between carboplatin alone and combination groups (Fig. 6F–I). Furthermore, no indications of normal tissue toxicity were noted at the tissue level upon analysis of H&E staining of liver, spleen, and femur bone marrow smears, evaluated by a board-certified pathologist (G.E. Sandusky; personal communication).

Discussion

The objective of the present study was to evaluate the outcome of modulating Mdm2 function in the context of current chemotherapeutic approaches for TNBC as well as assess Mdm2 as a therapeutic target. TNBCs are highly refractive to therapy and the development of multi-targeted treatments that exhibit an acceptable toxicity profile are needed. Approximately 60% of basal TNBCs bear mutations in p53 (15) and ~90% of mutations in p53 occur in the DNA binding domain. The MDA-MB-231 (mtp53 R280K), the MDA-MB-231 derivative TMD231 (mtp53 R280K) and the MDA-MB-468 (mtp53 R273H) cells used in our study all have missense mutations within the DNA binding domain of p53 (33). The mtp53 R280K mutation in the MDA-MB-231 and the TMD231 cells has been reported to have gain-of function properties (34); however, its exact role is still not well understood. Gain-of-function mutant p53 may antagonize other tumor suppressing capabilities of cells. In some cell types mtp53 can sequester p73, which leads to a blockade of p73-mediated downstream signaling (35). Xu and colleagues demonstrated that mutant p53 (mtp53) (R282W and R110P) exhibit a misfolded/aggregated state which leads to increased

aggregation of mtp53 with p73 causing inhibition of p73 function (35). It is not known if the gain-of-function ability of mutant p53 in the MDA-MB-231 and TMD231 (R280K) cells plays a similar role in co-aggregation with p73 and will be addressed in future studies. However, a sufficient pool of "free" p73 must exist for exposure of TNBC cells *in vitro* to combination Nutlin-3a/carboplatin treatment led to a synergistic inhibition of cell proliferation, which was dependent, at least in part, on p73α-mediated signaling (Figure 3B).

Previous studies have demonstrated that mutant p53 cancer cells can harbor nucleotide excision repair defects, rendering them highly sensitive to platinum agents (30). Furthermore, ongoing clinical trials for metastatic TNBC are including platinum agents in their treatment regimens (4, 36–38). In an orthotopic humanized breast-to-lung model, treatment with Nutlin-3a/carboplatin significantly inhibited primary tumor growth, and metastatic foci in the lung were fewer in number and smaller in size relative to treatment with vehicle or single-agent therapy. Pharmacokinetic studies have demonstrated efficient delivery of Nutlin-3a to the lungs, which was comparable to plasma levels (39). In addition, carboplatin is routinely used to treat non-small cell lung cancer, providing further rationale for the utility of this combination therapy to treat metastatic foci in the lung (40, 41). The p53 family member p73α has functions similar to p53 (17, 18, 42, 43), but is regulated differently by Mdm2. While p53 and p73α can both interact with Mdm2 in the same N-terminal hydrophobic pocket (12), Mdm2 does not ubiquitinate p73α (44–46). Rather, Mdm2 sequesters p73α thereby preventing downstream p73α-mediated signaling (45). Blockade of the binding of Mdm2 to p73α by Nutlin-3a increases the pool of p73α available to transcriptionally activate pro-apoptotic gene expression and promote apoptosis in mutant p53 and p53 null cells (12). TMD231 cells transfected with p73 siRNA were more resistant to carboplatin and Nutlin-3a/carboplatin compared siRNA control-transfected cells. Additionally, decreases in p73α protein levels via siRNA knockdown correlated with decreased Mdm2 protein in TMD231 cells. These data are consistent with previous reports indicating that p73α can directly bind to the Mdm2 promoter and increase Mdm2 gene expression (12, 47).

It has been previously demonstrated that Mdm2 binds directly to Nbs1 of the Mre11/Rad50/Nbs1 (MRN) complex, co-localizes with Nbs1 to DNA damage foci, and inhibits the DNA damage response (24, 25). While our studies do not demonstrate a direct interaction of chromatin-associated Mdm2 with the MRN complex, increases in Mdm2 associated chromatin following Nutlin-3a or combination Nutlin-3a/carboplatin are consistent with studies of Eischen and colleagues. They demonstrated that Nutlin-3a–induced increased levels of Mdm2 directly inhibit DNA damage response signaling and delayed DNA break repair in *p53*-null MEFs and in ovarian cancer cell lines that lacked p53 or that contained mutant p53 (48). Combination treatment and dosing strategies that reduce the amount of required chemotherapeutics are important clinically to decrease normal tissue toxicity as well as prevent the emergence of secondary malignancies caused by therapies that damage DNA. In MCF10A epithelial and human fibroblast cells, the combination treatment decreased cell growth *in vitro* compared to carboplatin alone but did not decrease cell growth beyond that of Nutlin-3a alone. In addition, the TMD231 cells were more sensitive

to the combination treatment than these other cell types. Jiang *et al*. previously reported that Nutlin-3 could protect renal cells from cisplatin-based therapy (49). To what extent Nutlin-3a provides chemoprotective effects in the present model will require further study.

The dosing schedule employed in the present breast-to-lung orthotopic model support the use of intermittent dosing schedules for Mdm2 inhibitors, particularly in the context of cytotoxic therapy. Bone marrow toxicity is one of the principal side effects of chemotherapeutic drugs and was monitored closely in the present *in vivo* studies. While there was a decrease in hematopoietic progenitor cells in the bone marrow of carboplatin- and Nutlin-3a/carboplatin-treated mice, the inclusion of Nutlin-3a did not lead to further increases in carboplatin-mediated toxicity. Analysis of normal tissues (liver, spleen, and bone marrow smears) by H&E indicated there were no obvious effects of the combination therapy on tissue integrity. Thus, combination Nutlin-3a/carboplatin treatment shows promise of efficacy with minimal effects on normal tissue toxicity compared to carboplatin-alone.

The optimized breast-to-lung orthotopic model described here can be used to test novel combination platinum-based regimens and further increase our understanding of how to therapeutically potentiate DNA damage in TNBC at primary and metastatic sites. The present studies demonstrate the promise of Mdm2 as a therapeutic target in combination with current therapeutic approaches for TNBC, and may lead to new clinical therapies for TNBC and metastases.

Supplementary Material

Refer to Web version on PubMed Central for supplementary material.

Acknowledgements

Research in this publication was supported by the National Cancer Institute of the National Institutes of Health under award number R01CA138798 (E. Tonsing-Carter, B.J. Bailey, H. Wang, L.D. Mayo, and K.E. Pollok); R01CA181204 (C.M. Eischen); the DeVault Fellowship-IUSCC Cancer Biology Training Program (E. Tonsing-Carter); pilot funding through the IUSCC Breast Cancer Program, the Vera Bradley Foundation, ITRAC, and the Indiana Clinical and Translational Sciences Institute (K.E. Pollok). We thank Courtney Hemenway (*In Vivo* Therapeutics Core), Malgorzata M. Kamocka, (Indiana Center for Biological Microscopy) Jenny Then, and Sydney Ross (Translational Research Integrated Biology Laboratory) for their expert assistance.

References

1. Schnitt SJ. Classification and prognosis of invasive breast cancer: from morphology to molecular taxonomy. Mod Pathol. 2010; 23(Suppl 2):S60–S64. [PubMed: 20436504]
2. Dent R, Trudeau M, Pritchard KI, Hanna WM, Kahn HK, Sawka CA, et al. Triple-negative breast cancer: clinical features and patterns of recurrence. Clin Cancer Res. 2007; 13:4429–4434. [PubMed: 17671126]
3. Fuertes MA, Castilla J, Alonso C, Perez JM. Cisplatin biochemical mechanism of action: from cytotoxicity to induction of cell death through interconnections between apoptotic and necrotic pathways. Curr Med Chem. 2003; 10:257–266. [PubMed: 12570712]
4. Villarreal-Garza C, Khalaf D, Bouganim N, Clemons M, Pena-Curiel O, Baez-Revueltas B, et al. Platinum-based chemotherapy in triple-negative advanced breast cancer. Breast Cancer Res Treat. 2014; 146:567–572. [PubMed: 25001611]

5. Hurley J, Reis IM, Rodgers SE, Gomez-Fernandez C, Wright J, Leone JP, et al. The use of neoadjuvant platinum-based chemotherapy in locally advanced breast cancer that is triple negative: retrospective analysis of 144 patients. Breast Cancer Res Treat. 2013; 138:783–794. [PubMed: 23542956]
6. Rayburn E, Zhang R, He J, Wang H. MDM2 and human malignancies: expression, clinical pathology, prognostic markers, and implications for chemotherapy. Curr Cancer Drug Targets. 2005; 5:27–41. [PubMed: 15720187]
7. Haupt Y, Maya R, Kazaz A, Oren M. Mdm2 promotes the rapid degradation of p53. Nature. 1997; 387:296–299. [PubMed: 9153395]
8. Araki S, Eitel JA, Batuello CN, Bijangi-Vishehsaraei K, Xie XJ, Danielpour D, et al. TGF-beta1-induced expression of human Mdm2 correlates with late-stage metastatic breast cancer. The Journal of clinical investigation. 2010; 120:290–302. [PubMed: 19955655]
9. Chen X, Qiu J, Yang D, Lu J, Yan C, Zha X, et al. MDM2 promotes invasion and metastasis in invasive ductal breast carcinoma by inducing matrix metalloproteinase-9. PloS one. 2013; 8:e78794. [PubMed: 24236052]
10. Vassilev LT, Vu BT, Graves B, Carvajal D, Podlaski F, Filipovic Z, et al. In vivo activation of the p53 pathway by small-molecule antagonists of MDM2. Science. 2004; 303:844–848. [PubMed: 14704432]
11. Ambrosini G, Sambol EB, Carvajal D, Vassilev LT, Singer S, Schwartz GK. Mouse double minute antagonist Nutlin-3a enhances chemotherapy-induced apoptosis in cancer cells with mutant p53 by activating E2F1. Oncogene. 2007; 26:3473–3481. [PubMed: 17146434]
12. Lau LM, Nugent JK, Zhao X, Irwin MS. HDM2 antagonist Nutlin-3 disrupts p73-HDM2 binding and enhances p73 function. Oncogene. 2008; 27:997–1003. [PubMed: 17700533]
13. LaRusch GA, Jackson MW, Dunbar JD, Warren RS, Donner DB, Mayo LD. Nutlin3 blocks vascular endothelial growth factor induction by preventing the interaction between hypoxia inducible factor 1alpha and Hdm2. Cancer research. 2007; 67:450–454. [PubMed: 17234751]
14. Soussi T, Beroud C. Assessing TP53 status in human tumours to evaluate clinical outcome. Nat Rev Cancer. 2001; 1:233–240. [PubMed: 11902578]
15. Shah SP, Roth A, Goya R, Oloumi A, Ha G, Zhao Y, et al. The clonal and mutational evolution spectrum of primary triple-negative breast cancers. Nature. 2012; 486:395–399. [PubMed: 22495314]
16. Dotsch V, Bernassola F, Coutandin D, Candi E, Melino G. p63 and p73, the ancestors of p53. Cold Spring Harbor perspectives in biology. 2010; 2:a004887. [PubMed: 20484388]
17. Jost CA, Marin MC, Kaelin WG Jr. p73 is a simian [correction of human] p53-related protein that can induce apoptosis. Nature. 1997; 389:191–194. [PubMed: 9296498]
18. Melino G, Bernassola F, Ranalli M, Yee K, Zong WX, Corazzari M, et al. p73 Induces apoptosis via PUMA transactivation and Bax mitochondrial translocation. J Biol Chem. 2004; 279:8076–8083. [PubMed: 14634023]
19. Helbig G, Christopherson KW 2nd, Bhat-Nakshatri P, Kumar S, Kishimoto H, Miller KD, et al. NF-kappaB promotes breast cancer cell migration and metastasis by inducing the expression of the chemokine receptor CXCR4. J Biol Chem. 2003; 278:21631–21638. [PubMed: 12690099]
20. Wiek C, Schmidt EM, Roellecke K, Freund M, Nakano M, Kelly EJ, et al. Identification of amino acid determinants in CYP4B1 for optimal catalytic processing of 4-ipomeanol. The Biochemical journal. 2015; 465:103–114. [PubMed: 25247810]
21. Oliver MH, Harrison NK, Bishop JE, Cole PJ, Laurent GJ. A rapid and convenient assay for counting cells cultured in microwell plates: application for assessment of growth factors. J Cell Sci. 1989; 92(Pt 3):513–518. [PubMed: 2592453]
22. Chou TC, Talalay P. Quantitative analysis of dose-effect relationships: the combined effects of multiple drugs or enzyme inhibitors. Adv Enzyme Regul. 1984; 22:27–55. [PubMed: 6382953]
23. Tallarida RJ. Quantitative methods for assessing drug synergism. Genes Cancer. 2011; 2:1003–1008. [PubMed: 22737266]
24. Alt JR, Bouska A, Fernandez MR, Cerny RL, Xiao H, Eischen CM. Mdm2 binds to Nbs1 at sites of DNA damage and regulates double strand break repair. J Biol Chem. 2005; 280:18771–18781. [PubMed: 15734743]

25. Bouska A, Lushnikova T, Plaza S, Eischen CM. Mdm2 promotes genetic instability and transformation independent of p53. Mol Cell Biol. 2008; 28:4862–4874. [PubMed: 18541670]
26. Braden WA, Lenihan JM, Lan Z, Luce KS, Zagorski W, Bosco E, et al. Distinct action of the retinoblastoma pathway on the DNA replication machinery defines specific roles for cyclin-dependent kinase complexes in prereplication complex assembly and S-phase progression. Mol Cell Biol. 2006; 26:7667–7681. [PubMed: 16908528]
27. Alt JR, Greiner TC, Cleveland JL, Eischen CM. Mdm2 haplo-insufficiency profoundly inhibits Myc-induced lymphomagenesis. EMBO J. 2003; 22:1442–1450. [PubMed: 12628936]
28. Cai S, Wang H, Bailey B, Ernstberger A, Juliar BE, Sinn AL, et al. Humanized bone marrow mouse model as a preclinical tool to assess therapy-mediated hematotoxicity. Clin Cancer Res. 2011; 17:2195–2206. [PubMed: 21487065]
29. Shea TC, Flaherty M, Elias A, Eder JP, Antman K, Begg C, et al. A phase I clinical and pharmacokinetic study of carboplatin and autologous bone marrow support. J Clin Oncol. 1989; 7:651–661. [PubMed: 2651580]
30. Sengupta S, Harris CC. p53: traffic cop at the crossroads of DNA repair and recombination. Nature reviews Molecular cell biology. 2005; 6:44–55. [PubMed: 15688066]
31. Smith ML. Mdm2 sensitizes MCF7 breast cancer cells to cisplatin or carboplatin. Breast Cancer Res Treat. 1999; 58:99–105. [PubMed: 10674873]
32. Terzian T, Suh YA, Iwakuma T, Post SM, Neumann M, Lang GA, et al. The inherent instability of mutant p53 is alleviated by Mdm2 or p16INK4a loss. Genes & development. 2008; 22:1337–1344. [PubMed: 18483220]
33. Junk DJ, Vrba L, Watts GS, Oshiro MM, Martinez JD, Futscher BW. Different mutant/wild-type p53 combinations cause a spectrum of increased invasive potential in nonmalignant immortalized human mammary epithelial cells. Neoplasia. 2008; 10:450–461. [PubMed: 18472962]
34. Hui L, Zheng Y, Yan Y, Bargonetti J, Foster DA. Mutant p53 in MDA-MB-231 breast cancer cells is stabilized by elevated phospholipase D activity and contributes to survival signals generated by phospholipase D. Oncogene. 2006; 25:7305–7310. [PubMed: 16785993]
35. Xu J, Reumers J, Couceiro JR, De Smet F, Gallardo R, Rudyak S, et al. Gain of function of mutant p53 by coaggregation with multiple tumor suppressors. Nature chemical biology. 2011; 7:285–295. [PubMed: 21445056]
36. O'Shaughnessy J, Osborne C, Pippen JE, Yoffe M, Patt D, Rocha C, et al. Iniparib plus chemotherapy in metastatic triple-negative breast cancer. N Engl J Med. 2011; 364:205–214. [PubMed: 21208101]
37. O'Shaughnessy J, Schwartzberg L, Danso MA, Miller KD, Rugo HS, Neubauer M, et al. Phase III study of iniparib plus gemcitabine and carboplatin versus gemcitabine and carboplatin in patients with metastatic triple-negative breast cancer. J Clin Oncol. 2014; 32:3840–3847. [PubMed: 25349301]
38. Carey LA, Rugo HS, Marcom PK, Mayer EL, Esteva FJ, Ma CX, et al. TBCRC 001: randomized phase II study of cetuximab in combination with carboplatin in stage IV triple-negative breast cancer. J Clin Oncol. 2012; 30:2615–2623. [PubMed: 22665533]
39. Zhang F, Tagen M, Throm S, Mallari J, Miller L, Guy RK, et al. Whole-body physiologically based pharmacokinetic model for nutlin-3a in mice after intravenous and oral administration. Drug Metab Dispos. 2011; 39:15–21. [PubMed: 20947617]
40. Okamoto H, Watanabe K, Kunikane H, Yokoyama A, Kudoh S, Asakawa T, et al. Randomised phase III trial of carboplatin plus etoposide vs split doses of cisplatin plus etoposide in elderly or poor-risk patients with extensive disease small-cell lung cancer: JCOG 9702. Br J Cancer. 2007; 97:162–169. [PubMed: 17579629]
41. Zukin M, Barrios CH, Pereira JR, Ribeiro Rde A, Beato CA, do Nascimento YN, et al. Randomized phase III trial of single-agent pemetrexed versus carboplatin and pemetrexed in patients with advanced non-small-cell lung cancer and Eastern Cooperative Oncology Group performance status of 2. J Clin Oncol. 2013; 31:2849–2853. [PubMed: 23775961]
42. Zawacka-Pankau J, Kostecka A, Sznarkowska A, Hedstrom E, Kawiak A. p73 tumor suppressor protein: a close relative of p53 not only in structure but also in anti-cancer approach? Cell Cycle. 2010; 9:720–728. [PubMed: 20160513]

43. Zhu J, Jiang J, Zhou W, Chen X. The potential tumor suppressor p73 differentially regulates cellular p53 target genes. Cancer research. 1998; 58:5061–5065. [PubMed: 9823311]

44. Dobbelstein M, Wienzek S, Konig C, Roth J. Inactivation of the p53-homologue p73 by the mdm2-oncoprotein. Oncogene. 1999; 18:2101–2106. [PubMed: 10321734]

45. Zeng X, Chen L, Jost CA, Maya R, Keller D, Wang X, et al. MDM2 suppresses p73 function without promoting p73 degradation. Mol Cell Biol. 1999; 19:3257–3266. [PubMed: 10207051]

46. Balint E, Bates S, Vousden KH. Mdm2 binds p73 alpha without targeting degradation. Oncogene. 1999; 18:3923–3929. [PubMed: 10435614]

47. Wang XQ, Ongkeko WM, Lau AW, Leung KM, Poon RY. A possible role of p73 on the modulation of p53 level through MDM2. Cancer research. 2001; 61:1598–1603. [PubMed: 11245471]

48. Carrillo AM, Hicks M, Khabele D, Eischen CM. Pharmacologically Increasing Mdm2 Inhibits DNA Repair and Cooperates with Genotoxic Agents to Kill p53-Inactivated Ovarian Cancer Cells. Molecular cancer research : MCR. 2015; 13:1197–1205. [PubMed: 25964101]

49. Jiang M, Pabla N, Murphy RF, Yang T, Yin XM, Degenhardt K, et al. Nutlin-3 protects kidney cells during cisplatin therapy by suppressing Bax/Bak activation. J Biol Chem. 2007; 282:2636–2645. [PubMed: 17130128]

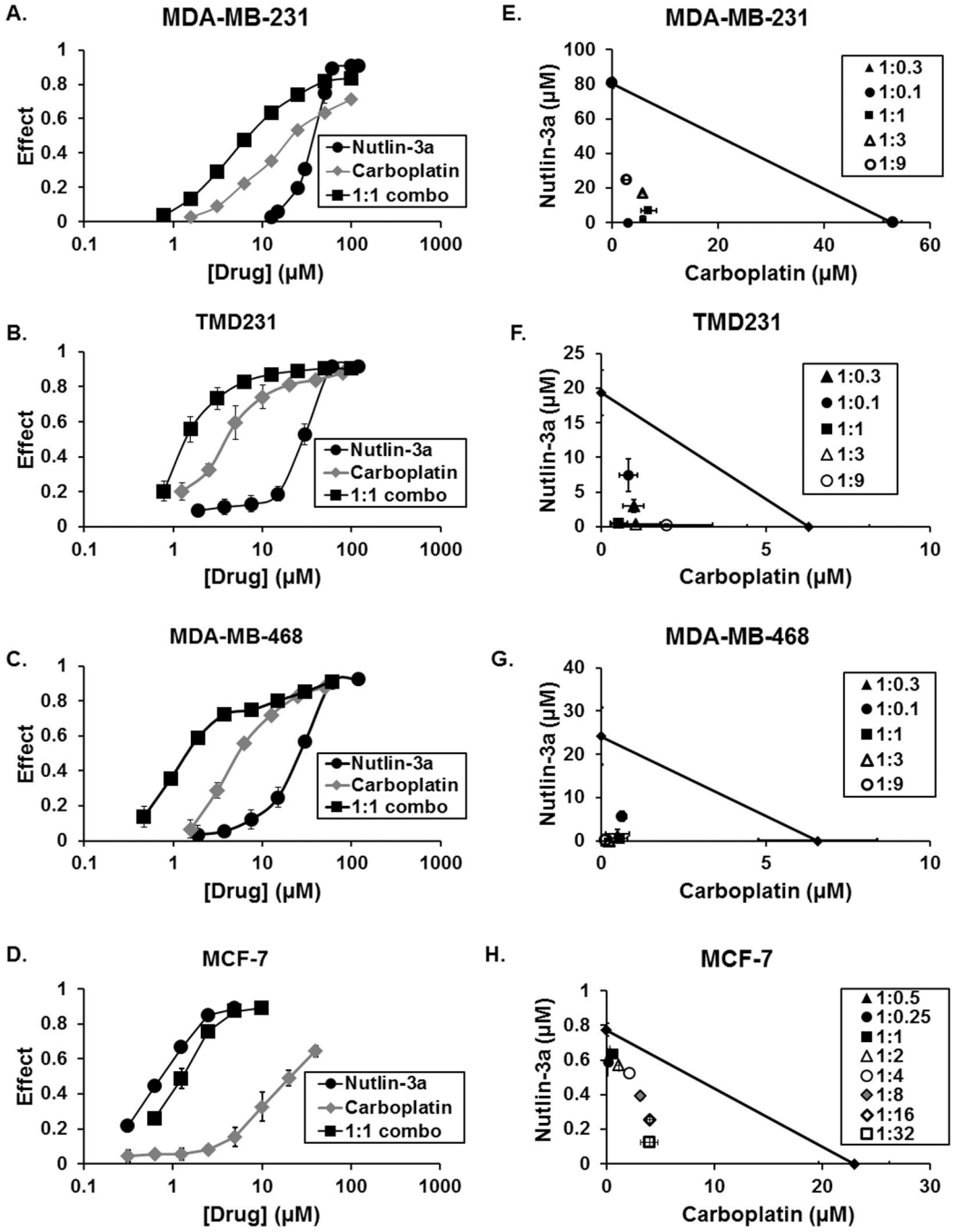

Figure 1. Nutlin-3a sensitizes TNBC cells to carboplatin-mediated DNA damage *in vitro*

(A–D) Dose-related inhibition of growth by carboplatin, Nutlin-3a, and the 1:1 combination in MDA-MB-231, TMD231 and MDA-MB-468 TNBC cells and MCF-7 breast cancer cells following 5 day proliferation assays. (E–H) IC_{50} values of carboplatin and Nutlin-3a were determined at the indicated dose-ratios and analyzed by isobolograms. Individual isobole points which lie below the diagonal line of additivity indicate synergism, points on the line indicate additivity, and points above the line indicate antagonism. Each point represents the

mean of three experiments. Vertical and horizontal lines indicate ±1 SD and are absent when less than the size of the point.

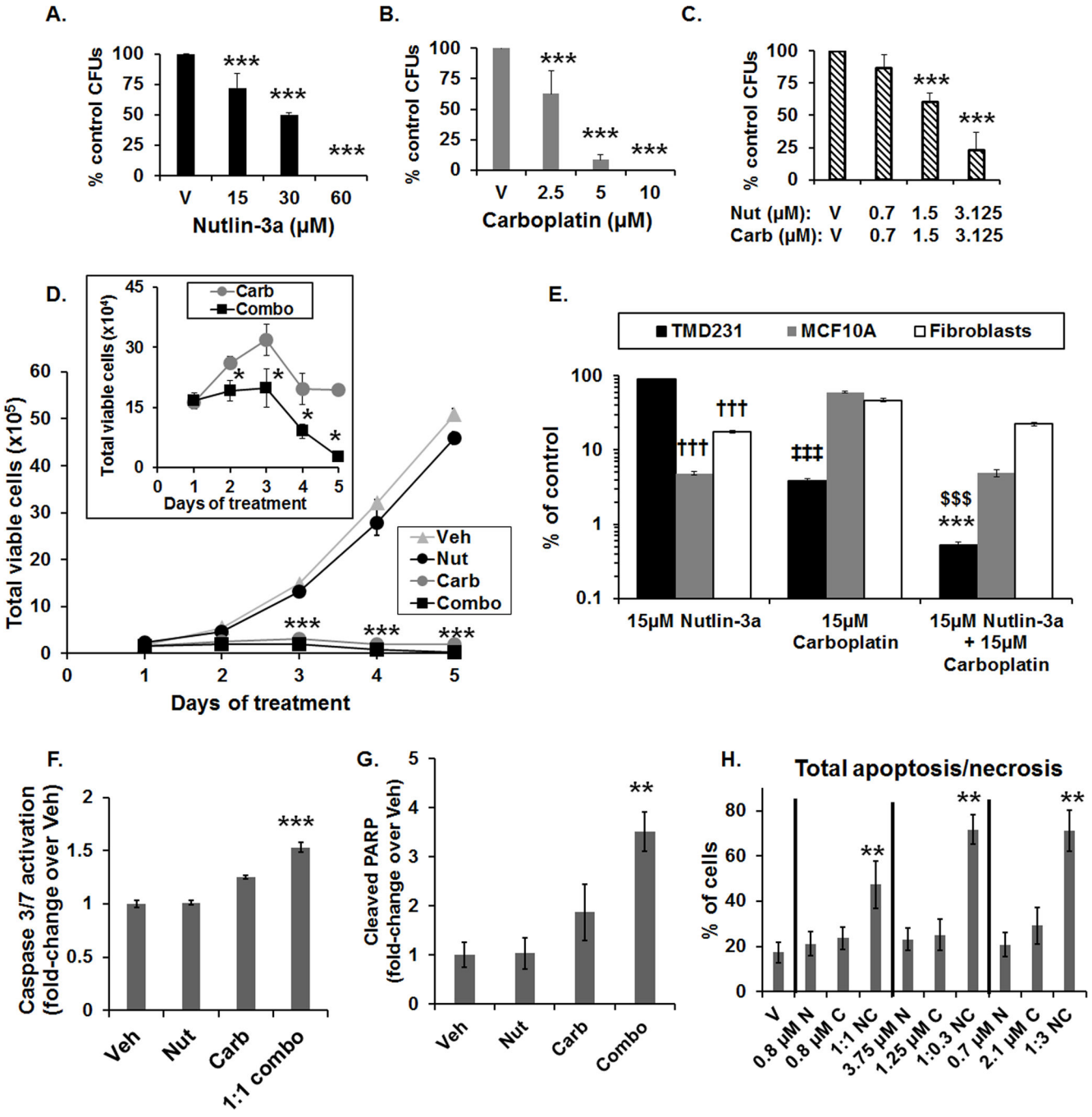

Figure 2. Potentiation of carboplatin-mediated DNA damage by Nutlin-3a increases cell death and differentially affects normal cells

(A–C) Dose-dependent reduction in colony forming units (CFUs) by Nutlin-3a (A), carboplatin (B), and in the 1:1 combination (C) (***p<0.001 vs V (vehicle), Holm-Sidak post hoc test, n=3). (D) Time-course of the number of viable TMD231 cells following treatment with vehicle (Veh), 15 μM Nutlin-3a (Nut), 15 μM carboplatin (Carb) or 1:1 combination (Combo) (***p<0.001 combination vs Vehicle, Holm-Sidak post hoc test, n=3). Inset: Number of viable cells following carboplatin and combination treatment (*p<0.05 vs carboplatin alone, Student's t-test, n=3). Vertical lines indicate ±1 SD and are

absent when less than the size of the point. (E) Effects of 15 μM of Nutlin-3a, carboplatin, or 1:1 combination in TMD231, MCF10A mammary epithelial, and human fibroblast cells on the number of viable cells, expressed as % of vehicle control, following 5-days of treatment. The y-axis was plotted on a log scale to better illustrate the comparisons. (††† $p<0.001$ vs TMD231 treated with 15 μM Nutlin-3a, ‡‡‡ $p<0.001$ vs MCF10A and fibroblasts treated with 15 μM carboplatin, $$$ $p<0.001$ vs MCF10A and fibroblasts treated with combination, ***$p<0.001$ vs TMD231 treated with 15 μM Nutlin-3a and carboplatin alone, Holm-Sidak post hoc test, n=3). (F) Activated Caspase-3/7 fold-induction in TMD231 cells treated with Vehicle (Veh), 15 μM Nutlin-3a (Nut), 15 μM carboplatin (Carb), or the combination (1:1 combo) for 3 days (***$p<0.001$ vs Veh, Nut, and Carb, Holm-Sidak post hoc test, n=3). (G) Cleaved PARP fold-induction in TMD231 cells treated with Vehicle (Veh), 15 μM Nutlin-3a (Nut), 15 μM carboplatin (Carb), or the combination (1:1 combo) for 3 days (***$p<0.01$ vs Veh, Student's t-test, n=3, ±SEM). (H) Total apoptosis/necrosis in TMD231 cells treated with Nutlin-3a (N), carboplatin (C), or the combination (NC) at the indicated doses and dose-ratios (**$p<0.01$ vs Veh, N, and C, Holm-Sidak post hoc test, n=3).

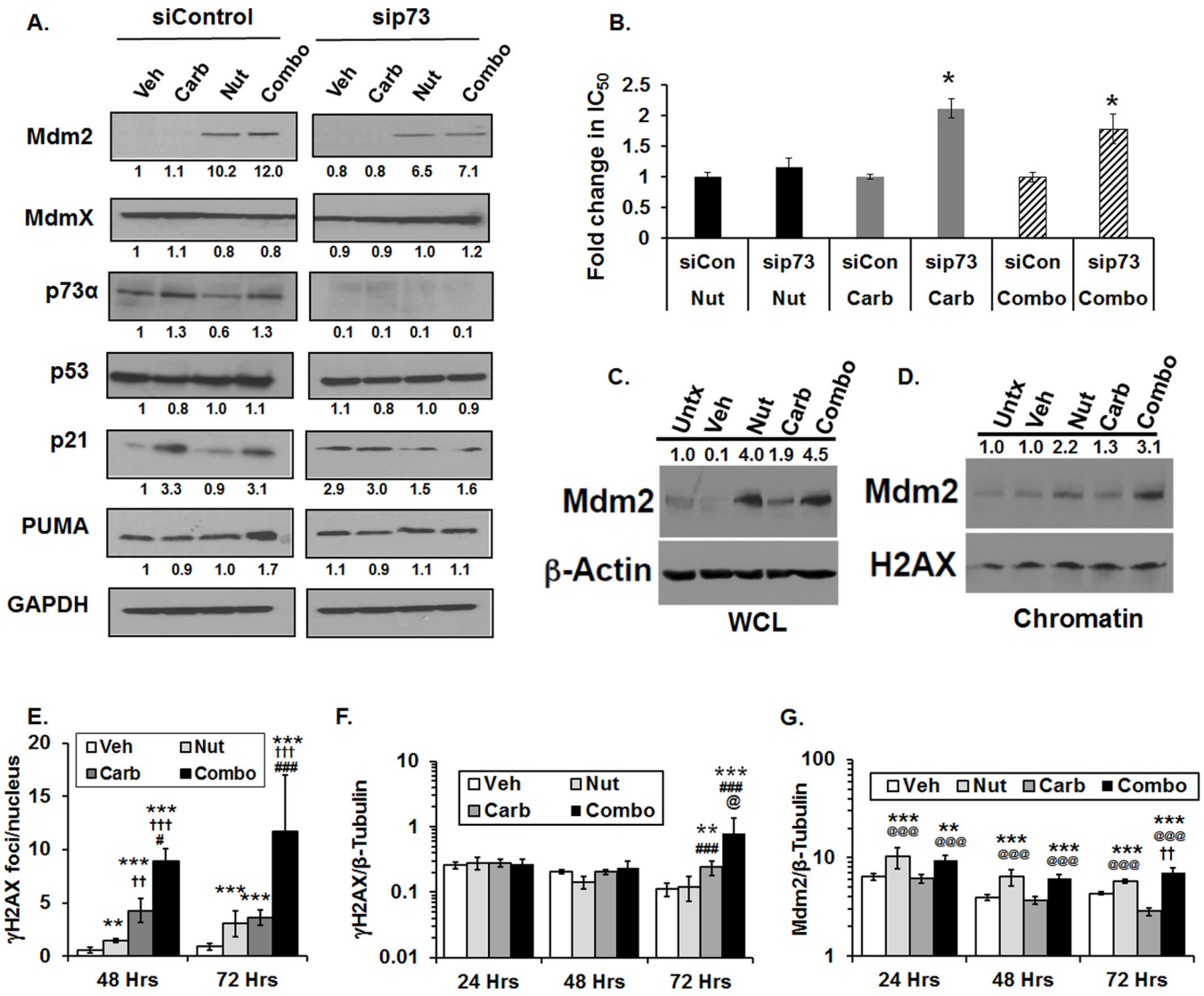

Figure 3. Effects of single agent and combination treatment on Mdm2 and dependency of treatment-mediated cell death on p73α

(A) TMD231 cells were transiently transfected with siControl or sip73 siRNA and treated with Vehicle (Veh), 15 μM Nutlin-3a (Nut), 15 μM carboplatin (Carb), or 1:1 combination (Combo) for 24 hours and levels of Mdm2, MdmX, p73α, p53, p21, PUMA, and GAPDH determined by Western blot. Densitometry for each protein was quantified by ImageJ and shown below each protein relative to siControl Vehicle-treated cells. (B) TMD231 cells transfected with sip73 or siControl (siCon) were treated with 15 μM Nutlin-3a (Nut), 15 μM carboplatin (Carb) or Nutlin-3a/carboplatin (Combo) for 3 days and IC_{50} values for inhibiting cell growth were determined after methylene blue staining (*$p<0.05$, vs siControl, Student's t-test, n=5 independent experiments). (C–D) Cells were not treated (Untx) or treated with Vehicle (Veh), 15 μM Nutlin-3a (Nut), 15 μM carboplatin (Carb), or 1:1 combination (Combo) for 6 hours. Mdm2 levels of (C) whole cell lysates (WCL) and the (D) chromatin fraction (Chromatin) were determined by Western blot. β-actin (WCL) and H2AX (chromatin) served as loading controls. Densitometry is shown above the blots. Data

are representative of 2 independent experiments. (E) γH2AX foci formation treated with Vehicle (Veh), 7.5 μM Nutlin-3a (Nut), 7.5 μM carboplatin (Carb), or 1:1 combination (Combo) (**p<0.01 vs Vehicle, ***p<0.001 vs Vehicle, ††p<0.01 vs Nut, †††p<0.001 vs Nut, #p<0.05 vs Carb, ###p<0.001 vs Carb at same time point, Holm-Sidak post hoc test, n=5 fields per group). (F) γH2AX levels normalized to β-Tubulin following Vehicle (Veh), 15 μM Nutlin-3a (Nut), 15 μM carboplatin (Carb), or 1:1 combination (Combo) in TMD231 cells (**p<0.01 vs Vehicle, ***p<0.001 vs Vehicle, ## p<0.015 vs Nut, ###p<0.001 vs Nut, and @p<0.01 vs Carb at the same time point, Holm-Sidak post hoc test, n=3 independent repeats). (G) Mdm2 levels normalized to β-Tubulin following Vehicle (Veh), 15 μM Nutlin-3a (Nut), 15 μM carboplatin (Carb), or 1:1 combination (Combo) in TMD231 cells (**p<0.01 vs Vehicle, ***p<0.001 vs Vehicle, @@@p<0.001 vs Carb, and ††p<0.01 vs Nut at the same time point, Holm-Sidak post hoc test, n=3 independent repeats).

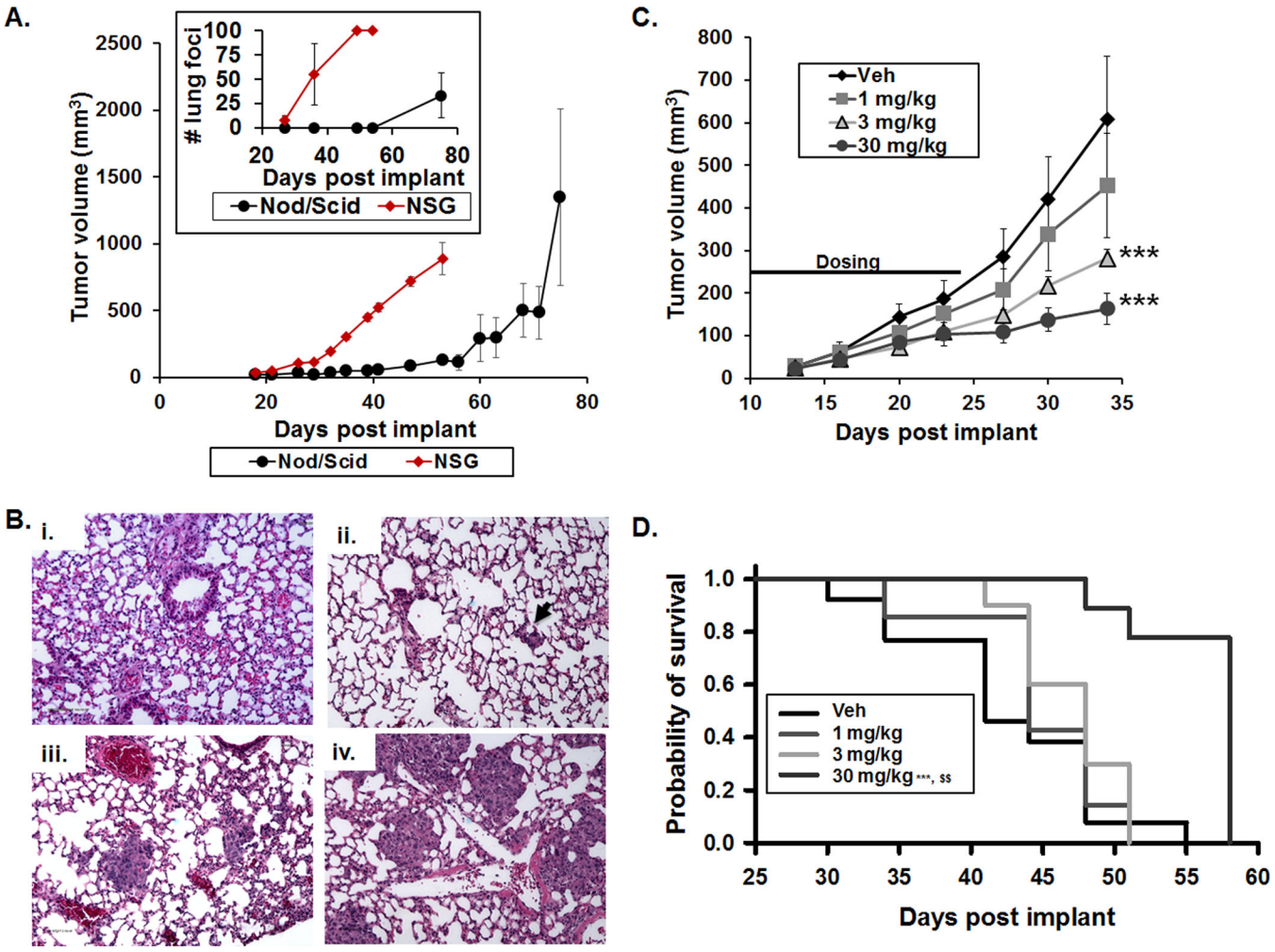

Figure 4. Metastatic breast-to-lung orthotopic model optimization and carboplatin dose-finding studies

Female Nod/Scid or NSG mice were implanted with 1×10^6 TMD231 cells in the mammary fat pad. (A) Longitudinal tumor growth in both mouse strains measured with calipers (±SEM). Inset: Number of lung metastatic foci in mice sacrificed at the indicated time points as determined by H&E staining (±SEM). (B) Representative microscopic images of H&E stained lung sections: normal mouse lung (i), days 18 (ii), 26 (iii), and 32 (iv) post-implantation of TMD231 cells. (C–D) NSG mice were implanted with 1×10^6 TMD231-CR cells and dosed with Vehicle (Veh), 1, 3, or 30 mg/kg carboplatin i.p. 3× per week for 2 weeks. (C) Dose-related decreases in tumor volume produced by carboplatin (***$p<0.001$ vs Vehicle, Holm-Sidak post hoc test, n=8–9 per group, ±SEM). (D) Dose-related increases in survival produced by carboplatin (***$p<0.001$ vs Vehicle, $$ $p<0.01$ vs 3 mg/kg, Holm-Sidak post hoc test, n=8–9 per group).

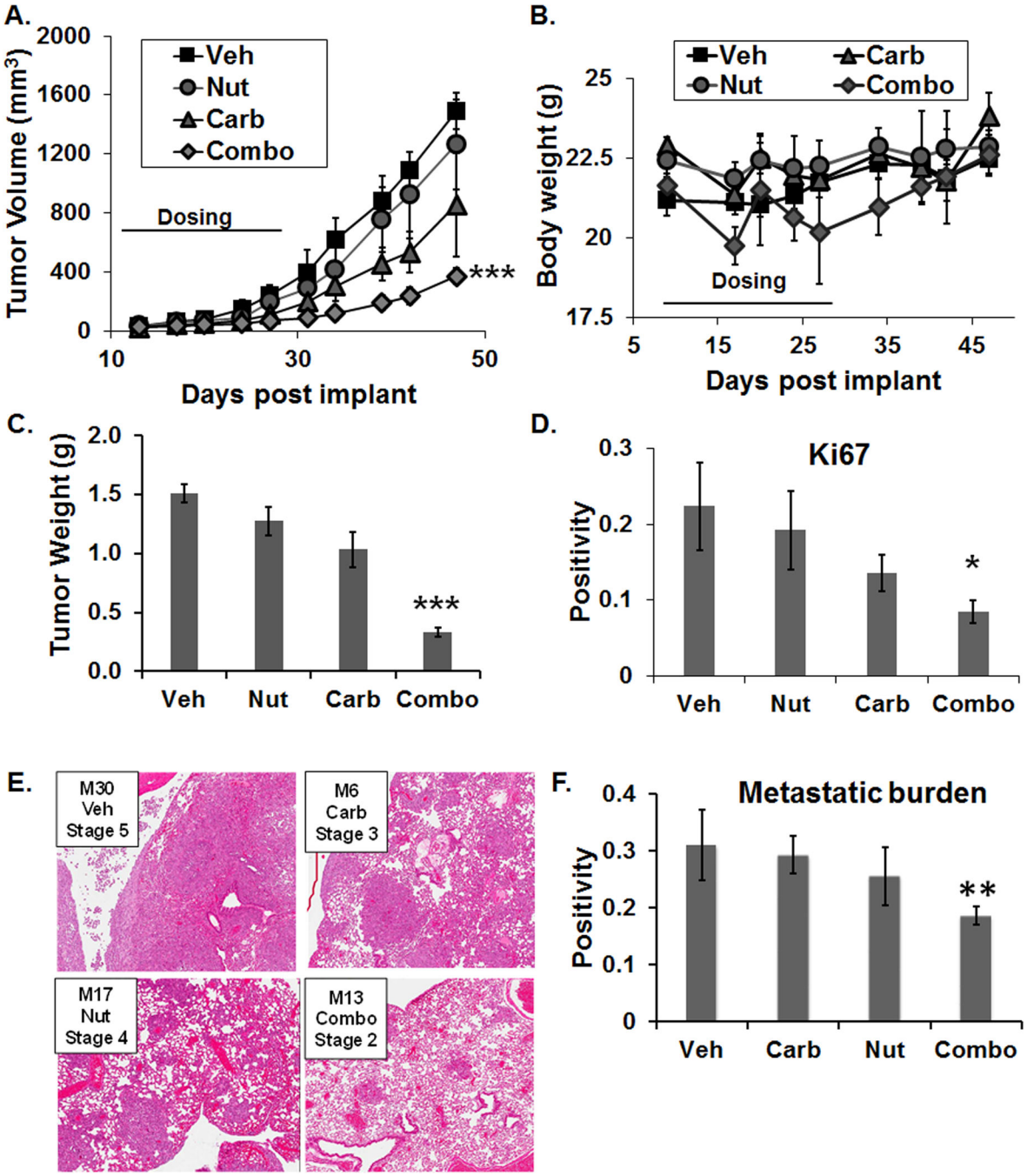

Figure 5. Carboplatin in combination with Nutlin-3a significantly decreases primary tumor growth and lung metastases

(A) Longitudinal tumor growth of mice administered Nutlin-3a (Nut), carboplatin (Carb) or the combination (Combo) (3× weekly for 2 weeks) (***$p<0.001$ vs all other groups, Holm-Sidak post hoc test, n=7–9 per group, ±SEM). (B) Body weights following drug treatment (±SEM). (C) Primary tumor weight at study termination (***$p<0.001$ vs all other groups, Holm-Sidak post hoc test, n=7–9 per group, ±SEM). (D) Ki67 staining positivity of primary tumors using whole slide digital imaging (*$p<0.05$ vs all groups, Holm-Sidak post hoc test). (E) Representative H&E stained lung sections (magnification 20×). (F) Metastatic burden as

measured by the proportion of the lungs positive for H&E staining at study termination using whole slide digital imaging (**p<0.01 vs all groups, Holm-Sidak post hoc test, n=5 per group).

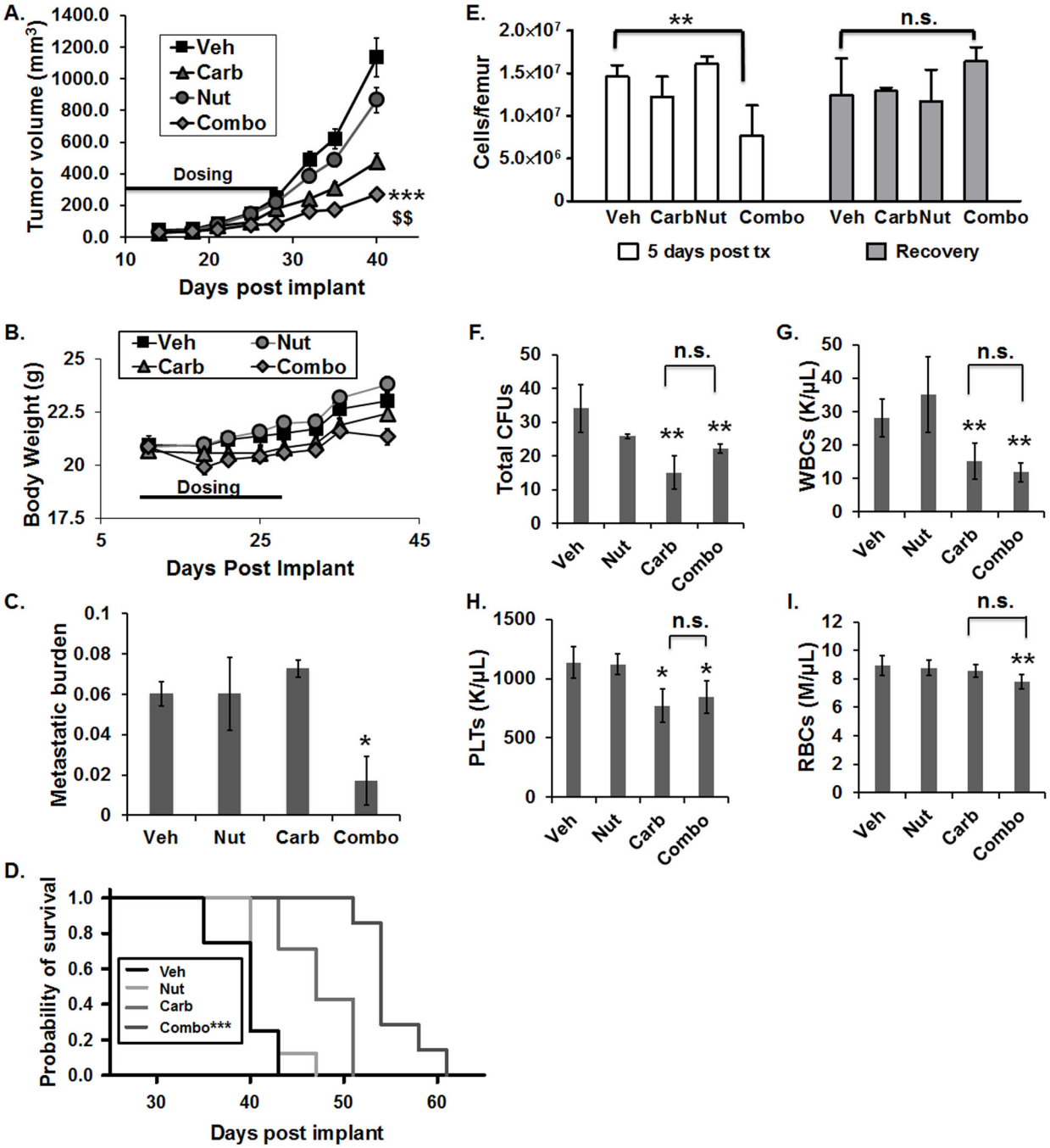

Figure 6. Carboplatin in combination with Nutlin-3a significantly decreases primary tumor growth and increases survival with minimal normal tissue toxicity

(A) Primary tumor volumes over time in Vehicle (Veh), 200 mg/kg Nutlin-3a (Nut), 20 mg/kg Carboplatin (Carb) and Nutlin-3a/carboplatin (Combo) treated mice. Treatment was administered 2 times weekly for 4 weeks (***p<0.001 vs Vehicle, $$ p<0.01 vs Nutlin-3a and carboplatin, n=12 per group at initiation of study, ±SEM). Note: Bone marrow was analyzed in some mice at 5 days post-treatment (n=4 per group); the remaining mice (n=8 per group) were monitored until the survival endpoint (≥800 mm^3) was met, at which time bone marrow was analyzed. (B) Body weights following drug treatment (±SEM) (C)

Metastatic burden as measured by H&E followed by whole slide digital imaging (*p<0.05 vs Veh, Holm-Sidak post hoc test, n=4 per group). (D) Probability of survival (***p<0.001 vs all other groups, n=8 per group). (E) Total bone marrow cells per femur determined either five days after the completion of treatment, (left panel, **p<0.01, Veh vs Combo, n=4 per group), or, after a period of recovery and when a mouse met the survival endpoint for tumor size (right panel, Veh vs Combo, n.s. (nonsignificant) p>0.05). Recovery phase varied depending on treatment group (Veh and Nut: 14 days, Carb: 18 days, and Combo: 28 days). (F–I) Normal tissue toxicity analysis of (F) total number of colony forming units (CFUs), (G) white blood cells (WBCs), (H) platelets (PLTs), and (I) red blood cells (RBCs) (*p<0.05 vs Vehicle, **p<0.01 vs Vehicle, n.s. p>0.05 carb vs combo, Holm-Sidak post hoc test, n=7–8 per group).